Available online at www.sciencedirect.com

ScienceDirect

Proceedings of the Combustion Institute 37 (2019) 1989–1996

Proceedings of the Combustion Institute

www.elsevier.com/locate/proci

Effect of stoichiometric mixture fraction on nonpremixed H_2–O_2–N_2 edge-flames

Zhenghong Zhou*, Siena S. Applebaum, Paul D. Ronney

Department of Aerospace and Mechanical Engineering, University of Southern California, Los Angeles, CA 90089-1453, USA

Received 1 December 2017; accepted 23 May 2018
Available online 21 June 2018

Abstract

The influences of stoichiometric mixture fraction (Z_{st}) and global strain rate (σ) on the shapes and propagation rates (U_{edge}) of nonpremixed edge-flames in H_2–N_2/O_2–N_2 mixtures were investigated using a counterflow slot-jet apparatus. Both positive and negative U_{edge} were observed depending on dilution level, Z_{st} and σ. At low Z_{st} only continuous flames were observed whereas at sufficiently high Z_{st}, where a shift from more oxygen-deficient to more fuel-deficient conditions at the reaction zone occurs, broken structures characteristic of low Lewis number premixed flames were observed which enabled combustion under conditions where no flames could be sustained at lower Z_{st}, even for the same dilution level. At sufficiently high σ these broken structures could transition from advancing edge-flames to isolated, stationary flames, particularly for highly-diluted mixtures. These findings were in surprisingly good agreement with theoretical predictions. Appropriate scalings of these behaviors for different mixtures based on computed 1D extinction strain rates were identified. Nonpremixed H_2–N_2/O_2–N_2 edge-flames have profoundly different responses to Z_{st} than corresponding hydrocarbon edge-flames, which is shown to be due to differences in the chemistry and Lewis numbers of the two fuels.

Keywords: Edge-flames; Lewis number; Mixture fraction; Nonpremixed flames; Counterflow

1. Introduction

"Edge-flames" [1,2] are transition regions between burning and non-burning portions of flame sheets that may exist in situations such as flames stabilized near a cold wall or splitter plate, leading edges of flames spreading across condensed-phase fuel surfaces, or flame sheets in highly turbulent flows where "holes" may open or re-seal [3]. Edge-flame behavior also strongly affects flame dynamics in forced unsteady Burke-Schumann configurations [4] and other flame stabilization scenarios [5]. The most significant property of an edge-flame is its propagation speed (U_{edge}), defined as the speed of the edge moving from the burned gases towards the unburned gases in the direction parallel to the flame sheet. Previous theoretical studies in premixed [6–8] and nonpremixed [9–11] configurations predict that edge-flames may propagate from

* Corresponding author.
E-mail address: zhenghoz@usc.edu (Z. Zhou).

https://doi.org/10.1016/j.proci.2018.05.010
1540-7489

the burning region into the unburned region, forming a "ignition front" with $U_{edge} > 0$ or retreat from the burning region into the burned region, forming an "extinction front" with $U_{edge} < 0$. U_{edge} is affected by factors including global strain rate (σ), Lewis numbers (Le, ratio of mixture thermal diffusivity to reactant mass diffusivity) of fuel and oxidant, heat losses, mixture strength and for nonpremixed edge-flames the stoichiometric mixture fraction $Z_{st} \equiv 1/(1+mX_f/X_o)$ where m is the stoichiometric oxygen-to-fuel mass ratio and X_f and X_o are the mass fractions of fuel and oxygen in the reactant mixture streams.

While pure fuel burning with highly-diluted oxygen (air) corresponds to low Z_{st} (typically 0.06 for hydrocarbon-air mixtures) is prevalent in traditional nonpremixed combustion, new fuels and combustion technologies (biofuels, oxyfuel combustion, massive exhaust gas recirculation, etc.) lead to much broader Z_{st} ranges (up to 0.8 for pure O_2 burning with highly-diluted hydrocarbon fuel and 0.93 for highly-diluted H_2.) In a counterflow, as Z_{st} increases the flame location moves from the oxidizer side of the stagnation plane to the fuel side, resulting in significant differences in the reactant temperature/composition/time history which in turn substantially affects burning rates as characterized by U_{edge} or extinction strain rate (σ_{ext}) [12–14]. For hydrocarbons, there are two competing factors. One is a chemical effect: at low Z_{st} the flame location is on the oxygen side of the stagnation plane and radicals produced primarily by the fuel must diffuse upstream to the reaction zone whereas at high Z_{st} the flame resides on the fuel side and radicals are readily convected downstream to the reaction zone, thereby strengthening the flame, consequently, σ_{ext} increases monotonically with Z_{st}. The other is a transport effect: at low Z_{st} reaction is O_2-limited whereas at high Z_{st} reaction is fuel-limited, leading to a shift in effective Le (Le_{eff}) from that of O_2 (Le_o) to fuel (Le_f) as Z_{st} increases. Hydrogen fuel has much lower Le_f than any hydrocarbon fuel and vastly different chemistry (we shall show hydrogen does not exhibit the same monotonic increase in σ_{ext} with Z_{st}), moreover, the very low Le_f of H_2 in O_2–N_2 mixtures may lead to diffusive-thermal instability (DTI) [15], particularly at high Z_{st}, which could lead to broken or cellular flames. While normally associated with premixed flames, DTI does occur in nonpremixed flames at near-extinction conditions when the more-consumed reactant has sufficiently low Le [16] and thus might be expected in H_2–N_2/O_2–N_2 edge-flames.

Since no systematic experimental study of nonpremixed hydrogen edge-flames has been conducted, this work examines nonpremixed H_2–N_2/O_2–N_2 edge-flame shapes, propagation rates, stability limits and extinction limits for varying Z_{st} (adjusted by changing the portion of N_2 on the H_2 side versus the O_2 side), varying σ (by changing flow rates) and varying mixture strengths (by changing N, defined as the moles of inert in the H_2:O_2:N_2 = 2:1:N mixture formed when fuel and oxidant streams are combined in stoichiometric proportions. For example, for N = 18 (H_2:O_2:N_2 = 2:1:18), if all N_2 flows from the fuel side then H_2:N_2 = 2:18 thus the fuel-side mixture is 10% H_2/90% N_2 and the oxygen-side mixture is 100% O_2, resulting in $Z_{st} = 0.9407$, whereas if all the N_2 flows from the O_2 side then H_2:N_2 = 2:0 thus the fuel-side mixture is 100% H_2 and the oxygen-side mixture is O_2:N_2 = 1:18 (5.26% O_2/94.74% N_2), resulting in $Z_{st} = 0.0074$. For these extreme Z_{st} cases and all intermediate Z_{st}, combining fuel and oxidant streams in stoichiometric proportions results in premixtures with H_2:O_2:N_2 = 2:1:18, all having the same premixed-flame properties). Following prior work [13,14] a counterflow slot-jet apparatus is employed which provides extensional strain orthogonal to the slot plane yet little convection along the slot length, thus edge-flame propagation speeds in the laboratory frame are essentially equal to the propagation speed relative to the cold unburned gas far ahead of the edge-flame (or behind, for retreating edge-flames).

2. Experimental apparatus, procedures and scaling

The counterflow slot-jet apparatus and procedures were similar to those employed previously [13,14]. Figure S1 shows a schematic of this apparatus. Slot-jet exit velocities (U_f and U_o for fuel and oxidizer respectively) were regulated by thermal mass flow controllers to achieve specified global strain rate ($\sigma = (U_f/d)[1+(U_o/U_f)(\rho_o/\rho_f)^{1/2}]$, where

Table 1
Properties of mixtures tested. S_L is calculated using CHEMKIN with Li et al. [22] kinetics. For all cases $Le_f \approx 0.33$ and $Le_o \approx 1.07$.

N	ρ_u/ρ_b	S_L (cm/s)	σ_{ext} (1/s) Z_{st} = 0.15	σ_{ext} (1/s) Z_{st} = 0.5	σ_{ext} (1/s) Z_{st} = 0.9
15	3.75	4.40	176.7	230.3	182.9
16	3.62	2.90	111.2	153.8	95.8
17	3.50	1.78	70.0	102.7	50.2
18	3.39	1.04	44.1	68.5	26.3
19	3.29	0.49	27.7	45.8	13.7
20	3.20	0.35	17.4	30.6	7.2

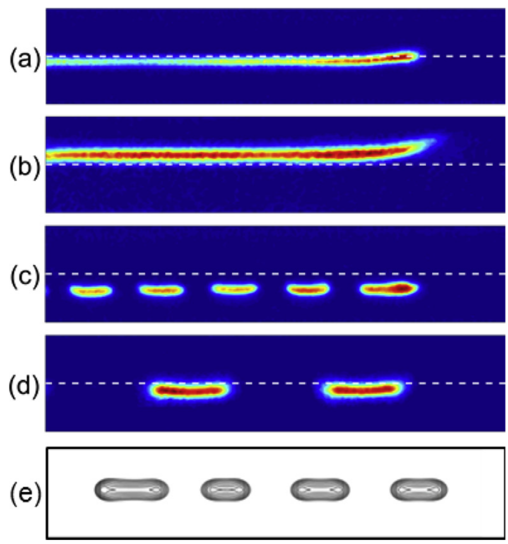

Fig. 1. False-color direct images of edge-flames in mixtures with N = 18. H_2–N_2 flows from the bottom upwards, O_2–N_2 from the top downwards. Slot spacing (d) = 7.5 mm. White dashed lines indicate the stagnation plane location. (a) $Z_{st} = 0.6$, $\sigma = 80$/s, advancing continuous-flame (mode I); (b) $Z_{st} = 0.4$, $\sigma = 80$/s, retreating continuous-flame (mode II); (c) $Z_{st} = 0.9$, $\sigma = 80$/s, advancing broken-flame (mode III) (d) $Z_{st} = 0.70$, $\sigma = 110$/s, stationary broken-flame (mode IV); (e) computed reaction rate contours for a mode III flame with $Le = 0.33$ [23].

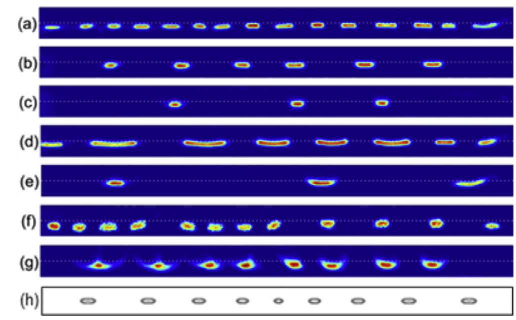

Fig. 2. False-color direct images of broken-flames. (a) N = 18, $Z_{st} = 0.8$, $\sigma = 100$/s; (b) N = 18.5, $Z_{st} = 0.8$, $\sigma = 100$/s; (c) N = 19, $Z_{st} = 0.8$, $\sigma = 100$/s; (d) N = 18, $Z_{st} = 0.7$, $\sigma = 100$/s; (e) N = 18, $Z_{st} = 0.7$, $\sigma = 120$/s; (f) N = 17, $Z_{st} = 0.9$, $\sigma = 20$/s; (g) N = 18, $Z_{st} = 0.85$, $\sigma = 240$/s; (h) computed reaction rate contours for a mode IV flame with $Le = 0.33$ [23]. Images (a) and (f) are advancing (Mode III), all others are stationary (Mode IV).

(ρ_o, ρ_f) are the gas densities at the jet exits and d the jet spacing [17]) and mixtures (H_2–N_2 and O_2–N_2) at values of X_o and X_f required to obtain desired values of Z_{st}. We employed equal jet exit velocities ($U_f = U_o$) and since $\rho_o \approx \rho_f$, the stagnation plane location was essentially at the midplane between the jets. For all cases shown H_2–N_2 issued from the lower jet and O_2–N_2 from the upper jet. Reversing these flows had no significant effect on the results, hence buoyancy effects were insignificant for the conditions tested. Honeycomb inserts at the jet exits provided uniform flow across the jets' width (5 mm) and length (130 mm). Nitrogen sheath flows with the same exit velocities as the reactive jets were employed on both sides of both reactant streams to prevent secondary flames. The jets were maintained at room temperature by water-cooling. The edge-flames were recorded with high-speed intensified video using a camera sensitive to near-IR emissions near 823 nm where H_2O has a weak emission band. U_{edge} and general flame behavior (broken vs. continuous, burning vs. extinguished) was cross-checked with shadowgraph images and no differences were found but only direct video images are reported here because of the challenges associated with interpreting shadowgraph images. Because the slot-jet aspect ratio is finite, there is a slight extensional flow along the slot length which influences U_{edge} in the laboratory frame slightly; following prior work [13,14], this bias was nullified by interpolating U_{edge} vs. position along the slot to the jet centerline. In some cases broken flame structures were observed which left nearly stationary flame "islands" behind the leading edge; we defined U_{edge} as the propagation speed of the leading flame island regardless of the behavior of the trailing flame islands. For retreating edge-flames this issue did not arise because broken flames were never observed. At jet Reynolds numbers $Re = U_{jet}d/\nu > 500$, where ν is the cold-gas kinematic viscosity, unsteady flames were observed, apparently indicating transition to turbulent flow, consequently, only data for $Re < 500$ are presented.

For conditions resulting in $U_{edge} > 0$, an N_2 jet was used to "erase" the established flame from one end of the slot-jet to nearly the other end and was then retracted, enabling the edge-flame to propagate. For conditions resulting in $U_{edge} < 0$, first a mixture with $U_{edge} > 0$ was introduced, then electrically-heated wires at both slot ends were activated and X_o and X_f were slowly reduced to the required values. (The heating wires anchored flames by enhancing local flame temperature and thus reaction rates at the flame ends under conditions which they would retreat without localized heating.) The N_2 jet was momentarily introduced at one slot end to separate the flame from its anchoring hot-wire, thereby triggering an extinction front.

Theories [9–11] predict that for adiabatic nonpremixed edge-flames with $Le_f = Le_o = 1$, constant density and low σ, $U_{edge}/S_L = 1$, where S_L is the laminar burning velocity of a stoichiometric mixture of fuel and oxidizer streams. Fundamentally this scaling is appropriate because for $Le_f \approx Le_o \approx 1$ the nonpremixed flame temperature is close to that of an adiabatic premixed flame and thus the over-

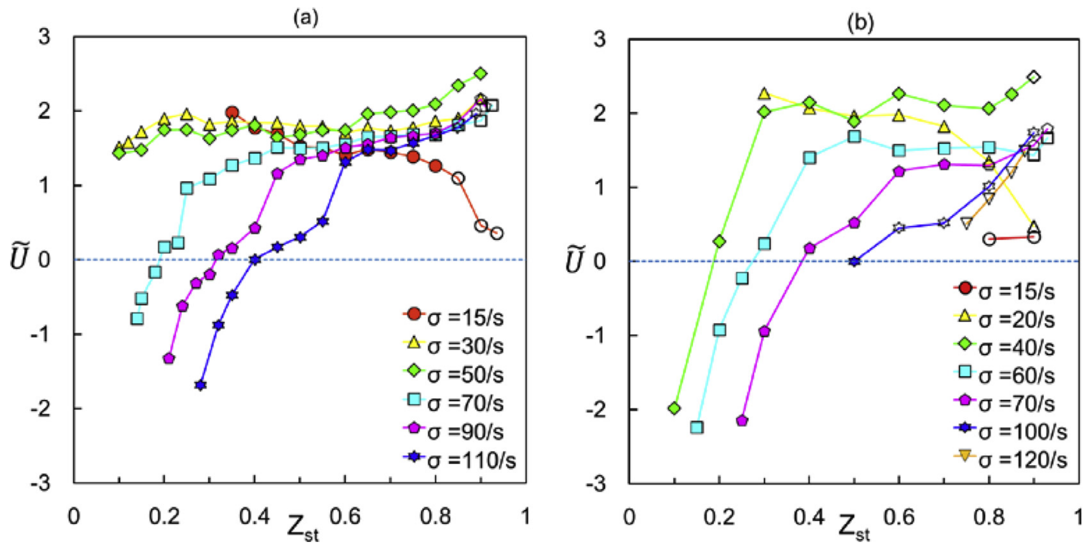

Fig. 3. Effect of Z_{st} and σ on scaled edge-flame speeds: (a) N = 17; (b) N = 18. Filled symbols indicate continuous flames (Mode I), open symbols indicate broken flames (Mode III).

all reaction rate ω can be estimated as $S_L{}^2/\alpha$ [15], where α is the gas thermal diffusivity. Other theory [18] predicts that when thermal expansion effects are incorporated, U_{edge}/S_L (in the unburned gas reference frame far upstream of the edge) increases in proportion to $(\rho_u/\rho_b)^{1/2}$, where ρ_u and ρ_b are the unburned and burned gas densities, respectively. Consistent with these theories, prior experiments [13,14] have shown that values of the scaled propagation speed $\tilde{U} = (U_{edge}/S_L)(\rho_u/\rho_b)^{-1/2}$ are near unity for nearly-adiabatic edge-flames with $Le_f \approx Le_o \approx 1$. In contrast, we found this scaling to be unsatisfactory for H_2–O_2–N_2 edge-flames because the low Le_f significantly enhances flame temperatures [19] and thus ω; in fact, for the mixtures we tested (Table 1) values of S_L are so low that they cannot burn as plane premixed flames in our apparatus (Peclet numbers $Pe \equiv S_L d/\alpha$ are below the typical extinction limit criterion $Pe = 40$, even for the least-diluted mixture). Park et al. [20] asserted that for weak H_2–O_2–N_2 flames the global extinction strain rate σ_{ext} rather than S_L may be used to characterize global reaction rates; following this approach U_{edge} will scale with $(\alpha\omega)^{1/2} \sim (\alpha\sigma_{ext})^{1/2}$ rather than S_L, thus, in this work we define $\tilde{U} = U_{edge}/[\alpha\sigma_{ext}(\rho_u/\rho_b)]^{1/2}$. We also scale σ with σ_{ext}, leading to a dimensionless strain rate $\varepsilon \equiv \sigma/\sigma_{ext}$. We shall show that $\tilde{U}$ and ε are indeed appropriate scalings; we also note they can be used for $Le_f \approx Le_o \approx 1$ since in that case $\sigma_{ext} \sim S_L{}^2/\alpha \sim \omega$ [15].

While low-S_L stretch-free flames can be extinguished by radiative loss, using the method described in [21], the estimated characteristic radiative loss rate is less than 0.35/s for all mixtures, which is far smaller than the smallest σ examined (16/s). Consequently, radiative transport is negligible compared to convective transport for our flames.

3. Results and discussion

3.1. Flame structures

Figure 1 shows false-color direct images of the four types of structures observed, denoted modes I-IV: (I) advancing continuous-flames, (II) retreating continuous-flames, (III) advancing broken-flames and (IV) stationary broken-flames. (No retreating broken flames were observed under any condition tested.) As expected, for Z_{st} less (greater) than 0.5, the flame lies on the O_2 (H_2) side of the stagnation plane. The broken flames are nearly flat, probably because the reaction zone must remain close to the stoichiometric mixing location, unlike low-Le cellular premixed flames which may be highly curved. The broken-flame structures are remarkably similar to those predicted theoretically (Fig. 1e) [23]. For Mode III, individual cells formed behind the leading edge-flame and remained stationary rather than splitting apart after formation of a continuous-flame, as predicted in [23]. A splitting sequence is shown in the Supplemental Data, Fig. S2. While advancing broken-flames (Mode III) would recover after being “erased” by the N_2 jet, stationary broken-flames did not recover after erasure.

Figure 2a–h show false-color direct images of broken-flames at high Z_{st}. Figure 2a-c show a sequence with increasing N where Z_{st} and σ are

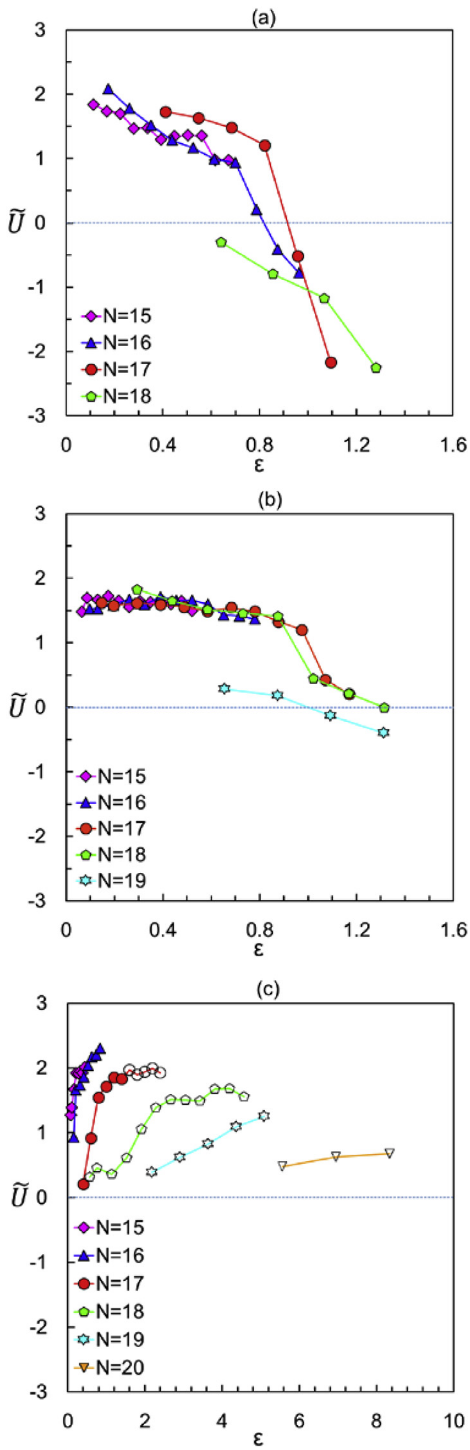

Fig. 4. Effect of scaled strain rate ε on scaled U_{edge}: (a) $Z_{st} = 0.15$; (b) $Z_{st} = 0.5$; (c) $Z_{st} = 0.9$. Filled symbols indicate continuous flames (Modes I, advancing and II, retreating), open symbols indicate broken flames (Modes III, advancing).

held constant; as N increases thus the mixture becomes weaker, the flame "void fraction" increases. Figure 2d,e show the same behavior with increasing σ where N and Z_{st} are held constant. Figure 2f shows a case with very low σ (near the heat-loss induced limit) with many irregular cells. Finally, Fig. 2g shows a case with very high σ, where the flow as seen by shadowgraph images (not shown) is clearly turbulent ($Re_{jet} > 500$) but the cells remain almost stationary. Stationary broken-flame structures (mode IV) are again remarkably similar to those predicted theoretically (Fig. 2h) [23].

3.2. Propagation rates

Figure 3 shows effects of Z_{st} and σ on scaled edge-flame speeds $\tilde{U}$ for two mixture strengths. It should be emphasized that for each plot, every point corresponds to exactly same mixture when fuel and oxidant streams are combined in stoichiometric proportions (thus every point on the plot has the same T_{ad}, ρ_u/ρ_b and S_L (see Introduction), yet $\tilde{U}$ (thus U_{edge}) varies drastically depending on Z_{st} and σ. As with nonpremixed hydrocarbon edge-flames [13], $\tilde{U}$ is maximum at intermediate σ with heat-loss induced extinction at low σ in addition to the high-σ extinction limit. Except at very high Z_{st}, $\tilde{U}$ increases with increasing Z_{st} which is consistent with the notion of decreasing Le_{eff} as Z_{st} increases (see Introduction). $\tilde{U}$ may exceed unity, consistent with the expectation of low Le_{eff} at high Z_{st}. It is somewhat surprising, however, that upon transition from advancing continuous (filled symbols, Mode I) to broken (open symbols, Mode III) edge-flames there is no significant change in $\tilde{U}$ values. Figure 4 shows effects of ε on $\tilde{U}$ for several dilution levels (N) for three fixed Z_{st} values. For low (0.15) and intermediate (0.5) Z_{st}, as ε increases $\tilde{U}$ first decreases slowly then decreases drastically until extinguishment. For high (0.9) Z_{st}, the trend is quite different, though in all cases have similar maximum scaled $\tilde{U}$ (1.5~2.5). The reason for this difference is discussed in the following section. In Fig. 4, all curves overlap except for near-extinction and broken-flame cases, demonstrating that ε and $\tilde{U}$ are proper scaling parameters for strain rate and edge-flame speed, respectively.

3.3. Regimes of flame behavior

Figure 5 shows maps of flame behavior in Z_{st}-ε space for two fixed N values. Note that on each map, every point produces the same stoichiometric mixture of fuel and oxidant streams. For all Z_{st} the two extinction limits at high and low ε are evident. For $Z_{st} < 0.6$ no broken flames are observed; only for $Z_{st} > 0.6$ can Modes I-IV all be observed as ε increases. For N = 17, $Z_{st} > 0.85$ and

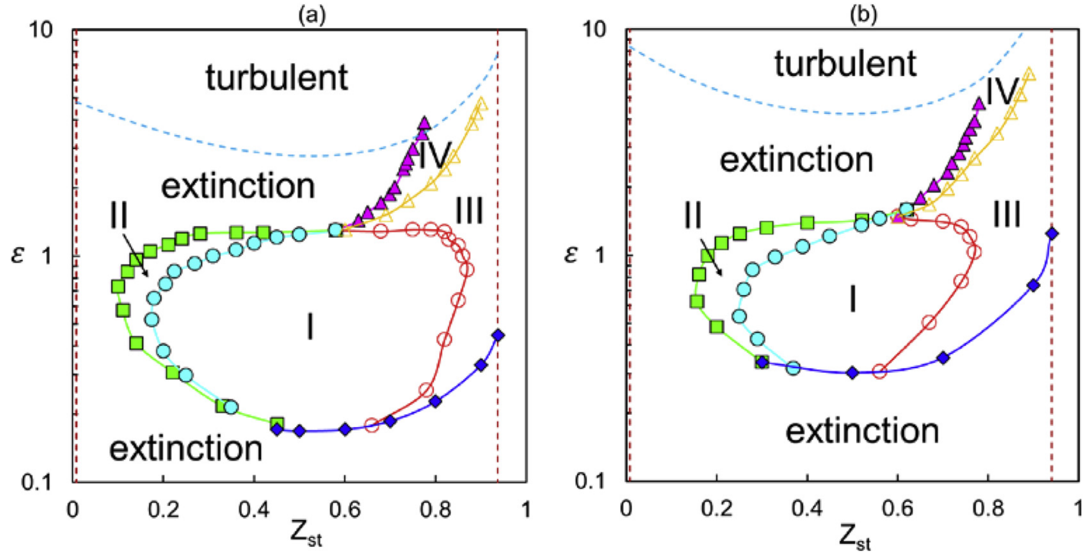

Fig. 5. Flame response maps in Z_{st}-ε space: (a) N = 17; (b) N = 18. Recall mode designations: (I) advancing continuous-flames, (II) retreating continuous-flames, (III) advancing broken-flames and (IV) stationary broken-flames. Vertical dashed lines indicate minimum (pure H_2 vs. O_2–N_2) and maximum (H_2–N_2 vs. pure O_2) values of Z_{st} attainable. Dashed curves indicate transition to turbulent structures.

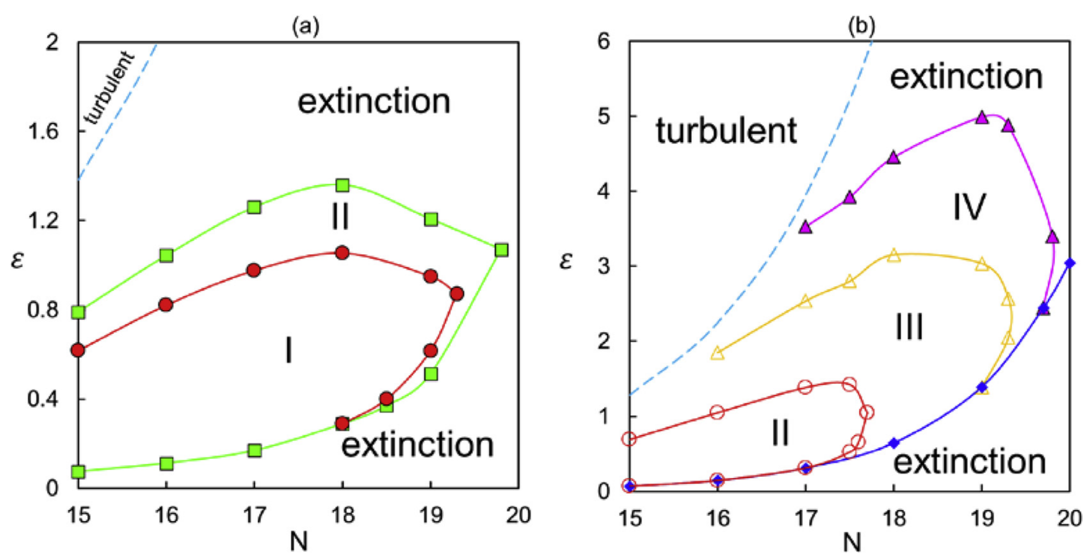

Fig. 6. Flame response maps in N-ε space: (a) $Z_{st} = 0.3$; (b) $Z_{st} = 0.8$. Dashed curves indicate transition to turbulent structures.

N = 18, $Z_{st} > 0.78$ only broken flames are observed, indicating dominance of low-*Le* DTI. For N = 17, $Z_{st} < 0.08$ and N = 18, $Z_{st} < 0.15$, no combustion occurs at any ε. Note that for both N = 17 and N = 18, at $Z_{st} \approx 0.58$, $\varepsilon \approx 1.3$, a rather remarkable bifurcation occurs - moving radially outward from these points small distances in Z_{st}-ε space, depending on the direction one may encounter any of 4 of the observed flame structures or extinction! Figure 6 shows maps of flame behavior in N-ε space for two fixed Z_{st} values. Again, the low-ε and high-ε extinction limits are evident and only for higher Z_{st} are broken flames observed.

3.4. Computations of σ_{ext} and comparison with experiment

Previous work [14] on Z_{st} influences on non-premixed edge-flames in hydrocarbon fuels demonstrated that many aspects of multidimensional

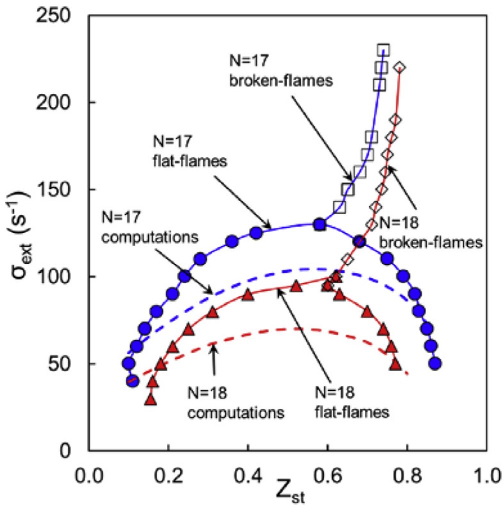

Fig. 7. Comparison of measured (solid lines and data points) and computed (dashed curves) values of extinction strain rate (σ_{ext}) for varying Z_{st} with N = 17 and N = 18.

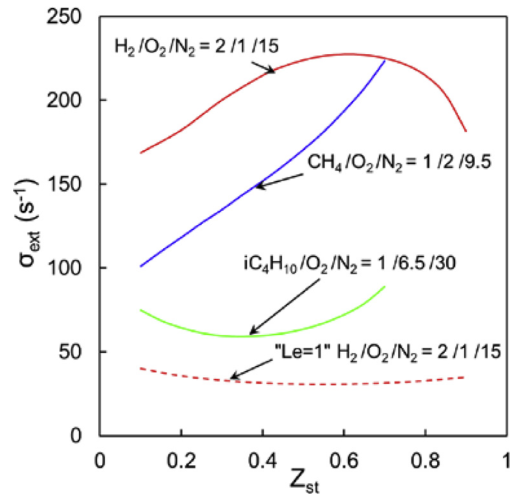

Fig. 8. Computed effects of Z_{st} on σ_{ext} for H_2–N_2/O_2–N_2 mixtures with standard transport and artificial transport causing $Le_f = Le_o \approx 1$, along with results for CH_4–N_2/O_2–N_2 ($Le_f = Le_o \approx 1$) and i-CH_4–N_2/O_2–N_2 ($Le_f > Le_o \approx 1$) mixtures.

edge-flame behavior could be interpreted in terms of the readily-computed σ_{ext}. Such computations (Fig. 7) for H_2–N_2/O_2–N_2 flames were performed with CHEMKIN using the same gap (d) as the experiments. Measured values of σ_{ext} are similar to but mostly higher than the computed values. For $Z_{st} > 0.6$, two sets of experimental data are shown, for "extinction" of continuous-flames (transition to broken-flames) and for extinction of broken-flames. Remarkably, computed values of σ_{ext} correspond well with transition to broken-flames observed in experiments. Values of σ at extinction of broken-flames increase rapidly with increasing Z_{st} and at $Z_{st} > 0.8$ could not be observed because of transition to turbulent flow (see Fig. 5). Figure 7 again illustrates the bifurcation in flame behavior near $Z_{st} \approx 0.6$. This bifurcation in the experiment data is due to transition from one-dimensional continuous to multi-dimensional broken-flame structures, whereas the computations are strictly one-dimensional and cannot exhibit this bifurcation. Ref. [23] reports computations employing schematic single-step chemistry and predicts that that broken-flames exist only when continuous flames cannot, which is precisely what is seen experimentally. It is unclear whether the peak in σ_{ext} that occurs at $Z_{st} \approx 0.6$ is fundamentally related to this bifurcation or is purely coincidental.

As discussed in the Introduction, Z_{st} influences on nonpremixed edge-flames in hydrocarbon fuels are affected by both Lewis numbers of fuel and oxygen and the unique chemistry of these fuels [14]. To separate Le and chemistry effects for hydrogen, computations of σ_{ext} were performed with Lennard–Jones parameters and molecular masses of H_2 and H set to those of O_2 and O, respectively, in order to force the Lewis numbers of H_2 and O_2 to be equal (and both nearly unity). Comparisons of H_2–N_2/O_2–N_2 flames with standard transport and artificial transport causing $Le_f = Le_o \approx 1$ are shown in Fig. 8. With $Le_f = Le_o \approx 1$, σ_{ext} decreases by a factor of 4,5 and becomes almost independent of Z_{st}. By comparing these data with CH_4–N_2/O_2–N_2 flames which also have $Le_f = Le_o \approx 1$ but the unique hydrocarbon chemistry that leads to σ_{ext} monotonically increasing with Z_{st}, (also shown in Fig. 8) it can be concluded that (1) the low Le of H_2 causes more robust flames with higher σ_{ext} and (2) Le_f effects, not chemistry effects, are responsible for the non-monotonic effect of Z_{st} on σ_{ext} in H_2–N_2/O_2–N_2 flames. Figure 8 also shows results for i-C_4H_{10}–N_2/O_2–N_2 mixtures where (in contrast to H_2–N_2/O_2–N_2) the high Le_f of i-C_4H_{10} causes a decrease in Le_{eff} (from Le_f to Le_o) as Z_{st} decreases, and thus exhibits non-monotonic behavior in contrast to the monotonic trend with CH_4–N_2/O_2–N_2 mixtures.

4. Conclusions

The effects of stoichiometric mixture fraction (Z_{st}) on flame structure and propagation rates in nonpremixed edge-flames H_2–N_2/O_2–N_2 mixtures were studied using a counterflow slot-jet apparatus. Both advancing and retreating edge-flames were characterized in terms of scaled edge-flame speed ($\tilde{U}$) and strain rate (ε). Due to the low Lewis number of H_2, scalings of $\tilde{U}$ and ε based on burning velocity S_L were inappropriate, instead scalings based on extinction strain rate σ_{ext} were successfully employed. Both high-ε residence-time limit extinction limits and low-ε heat loss-induced extinction limits were observed. As in prior work on hydrocarbon edge-flames [14], $\tilde{U}$ is neither independent of Z_{st} nor symmetric with respect to $Z_{st} = 0.5$, but for very different reasons. For hydrocarbons a chemical effect leads to $\tilde{U}$ monotonically increasing with Z_{st}, but this effect is absent in H_2–N_2/O_2–N_2 flames. Instead, the low Lewis number of H_2 and the shift from oxygen-limited to fuel-limited reaction as Z_{st} increases causes the observed behavior. Above $Z_{st} \approx 0.6$ a bifurcation leads to the possibility of broken (in many cases still nearly planar) edge-flames which may be advancing or stationary, but were not observed for retreating edges. The broken flames continue to survive under conditions (high strain or heat loss) where continuous plane edge-flames cannot. These results indicate that the behavior of turbulent nonpremixed hydrogen flames and the effects of stoichiometric mixture faction thereupon should not be anticipated based on extrapolation of Lewis number and strain rate effects for flames in hydrocarbons or other fuels.

Acknowledgments

The authors are grateful to Hang Song for his help with the experiments. This work was supported by the U.S. National Science Foundation, grant CBET-1236892.

Supplementary materials

Supplementary material associated with this article can be found, in the online version, at doi:10.1016/j.proci.2018.05.010.

References

[1] J.D. Buckmaster, *Prog. Energy Combust. Sci.* 28 (2002) 435–475.
[2] S.H. Chung, *Proc. Combust. Inst.* 31 (2007) 877–892.
[3] S. Karami, E.R. Hawkes, M. Talei, J.H. Chen, *Combust. Flame* 169 (2016) 110–128.
[4] N. Magina, T. Lieuwen, *Combust. Flame* 167 (2016) 395–408.
[5] T.C. Lieuwen, *Unsteady Combustor Physics*, Cambridge University Press, 2012.
[6] R. Daou, J. Daou, J. Dold, *Proc. Combust. Inst.* 29 (2002) 1559–1564.
[7] R. Daou, J. Daou, J. Dold, *Combust. Theory Model.* 7 (2003) 221–242.
[8] J. Daou, A. Linan, *Combust. Flame* 118 (1999) 479–488.
[9] J.D. Buckmaster, *Combust. Sci. Tech.* 115 (1996) 41–68.
[10] J. Daou, A. Liñán, *Combust. Theory Model.* 2 (1998) 449–477.
[11] R. Daou, J. Daou, J. Dold., *Combust. Theory Model.* 8 (2004) 683–699.
[12] R. Chen, R.L. Axelbaum, *Combust. Flame* 142 (2005) 62–71.
[13] M.S. Cha, P.D. Ronney, *Combust. Flame* 146 (2006) 312–328.
[14] H. Song, P. Wang, R. Boles, D. Matinyan, H. Prahanphap, J. Piotrowicz, P.D. Ronney, *Proc. Combust. Inst.* 36 (2017) 1403–1409.
[15] F.A. Williams, *Combustion Theory*, Cummins, Benjamin, 1985.
[16] R.-H. Chen, G.B. Mitchell, P.D. Ronney, *Proc. Combust. Inst.* 24 (1992) 213–221.
[17] K. Seshadri, F.A. Williams, *Int. J. Heat Mass Trans.* 21 (1978) 251–253.
[18] G. Reutsch, L. Vervisch, A. Liñán, *Phys. Fluids* 7 (1995) 1447–1454.
[19] C.K. Law, S.H. Chung, *Combust. Sci. Tech.* 29 (1982) 129–145.
[20] O. Park, P. Veloo, H. Burbano, F.N. Egolfopoulos, *Combust. Flame* 162 (2015) 1078–1094.
[21] P.D. Ronney, *Proc. Combust. Inst.* 27 (1998) 2485–2506.
[22] J. Li, Z. Zhao, A. Kazakov, F.L. Dryer, Int. J. Chem. Kinetics 36 (2004) 566575.
[23] R.W. Thatcher, J.W. Dold, *Combust. Theory Model.* 4 (2000) 435–457.

The Combustion Institute
5001 Baum Boulevard, Suite 644
Pittsburgh, Pennsylvania 15213-1851 USA
Ph: (412) 687-1366 Fax: (412) 687-0340
Office@CombustionInstitute.org CombustionInstitute.org

16 January 2019

Professor Zhenghong Zhou
University of Southern California

Dear Prof. Zhou:

It is our great pleasure to inform you that your manuscript ***Effect of stoichiometric mixture fraction on nonpremixed H_2–O_2–N_2 edge-flames*** has been selected as the Distinguished Paper in the Laminar Flames for the 37th International Symposium on Combustion. Congratulations on this achievement and please, reach out to your co-authors to share the good news!

An announcement of your selection will be posted on The Combustion Institute (CI) website and included in our quarterly newsletter. Elsevier has granted permission for your paper to be available as a free PDF download during February – April 2019 for all members. We will also list the authors for all 13 Distinguished Papers on the awards page of the CI website. This will increase the visibility of your work and the importance of the research scope within your field of combustion science.

We ask that you provide us with the **exact spelling of yourself and your co-authors** in the manner you prefer to see it displayed, and your **confirmed mailing addresses**, so that we may send your certificates. Please email these items to The Combustion Institute at: Office@CombustionInstitute.org. In the next several weeks, we will be requesting additional details of your research to publicize information to our members about this paper.

The Distinguished Paper Award makes you a candidate for the Silver Combustion Medal. The Silver Combustion Medal Committee will review the Distinguished Papers to select the top manuscript. The Silver Combustion Medal will be announced to the CI membership at the 38th Symposium on Combustion in Adelaide, Australia.

Congratulations,

Heinz Pitsch and Hai Wang
Program Co-Chairs, 37th International Symposium on Combustion